出國報告（出國類別：參加國際會議）

「PROTECT2009 - 第二屆結構與材料在衝擊與爆炸荷重下」國際會議

服務機關：海軍軍官學校
姓名職稱：任展勇助理教授

派赴國家：日本
出國期間：98 年 8 月 19 日至 98 年 8 月 21 日
報告日期：98 年 10 月 31 日

摘　要

在現代土木工程中，大跨度及高樓層的新型結構物不斷的出現，對工程材料的強度、韌性等亦有了更高的要求，因此高強度混凝土或高性能混凝土的應用也越來越廣泛。而活性粉混凝土爲近年來發展出來的超高強鋼纖維混凝土材料，優異之材料性質兼顧了高強度及高性能等特性，並在添加少量之鋼纖維後，可有效提高抗拉及抗彎強度、耐衝擊性和韌性。因此，本研究針對鋼纖維超高強混凝土之動態特性利用分離式哈普金森壓桿進行高應變率實驗，了解其在不同應變率下的動態力學及能量損耗的性質，研究結果顯示在不同衝擊速度下，材料之動態強度將隨著應變率的增加而增加，其中以不含鋼纖維之試體動態增強因子較爲顯著。而對於動態能量損耗的性質則與纖維的含量成正比。

目　次

參加會議目的

第二 屆 Performance, Protection & Strengthening of Structures under Extreme Loading 是由日本防衛大學所主辦，會議於 2009 年 8 月 19 至 21 日在神奈川縣橫須賀市之湘南度假中心(Shonan Village Center)舉行，主要是針對結構與材料在衝擊與爆炸荷重下之各項特性研究進行發表，藉以提升國際上相關領域之科技及學術水準，爲目前有關結構與材料動態特性領域之重要國際會議之一。參加之學者專家包含各國大學研究單位、重要企業機構及科技研發單位，可謂十分踴躍，藉由參加多場學術演講與壁報觀摩，吸收新知，瞭解國際間目前在基礎科學、應用工程、結構防護、碰撞以及爆震工程之研究趨勢與方向，獲益良多。

參加會議過程

本次會議-Performance, Protection & Strengthening of Structures under Extreme Loading 是由日本防衛大學所主辦，會議於 2009 年 8 月 19 至 21 日在神奈川縣橫須賀市之湘南度假中心(Shonan Village Center)舉行，主要是針對結構與材料在衝擊與爆炸荷重下之各項特性研究進行發表，藉以提升國際上相關領域之科技及學術水準，爲目前有關結構與材料動態

特性領域之重要國際會議之一。參加之學者專家包含各國大學研究單位、重要企業機構及科技研發單位，可謂十分踴躍。

本次會議之論文皆以口頭報告方式，會議論文之主題包括：

結構效能

- Impact Loads
- Blast and Explosive Loads
- Shock Loads
- Fire
- Seismic Loads

動態荷重下結構補強

- Assessment of Structural Condition
- Coatings and Surface Treatments
- Strengthening and Repair Methods
- Retrofitting for Seismic Loads

材料性能

- Constitutive Response under High Strain-Rates
- Influence of Low and High Temperatures
- Cyclic and Other Dynamic Loads
- Test Methods, Standardization and Performance Criteria
- Specialized Materials including Fiber Reinforced and High Performance Concrete, Specialized Steels and Fiber Reinforced Polymers

結構管理與存活性

- Protection Concepts and Designs
- Underground Facilities
- Structural Health Monitoring and Advanced Sensing

大會於 8 月 19 日上午舉行開幕典禮，首先由大會主席，亦即日本防衛大學土木與環境工程系教授 Dr. Y. Sonoda 致歡迎詞後，隨即由加拿大

卑詩大學之 Dr. Mindess 與英國曼徹斯特大學之 Dr. Wang 分別針對纖維強化混凝土受衝擊荷重之研究以及歐洲近年來對鋼與複合結構耐火性能研究之發展進行專題演講。之後隨即進行論文之發表與討論，每場次報告及討論之時間爲三十分鐘，各場次均十分踴躍，尤其是在衝擊與爆震相關領域之討論。

與會心得

由於本會議爲國際研究結構防護及碰撞以及爆震工程應用之研討會，本會議約有二百餘位國際知名之人士參加，大多爲歐美人士，亞洲則以日本及中國的學者較多。本次會議中筆者將對於結構在高速重複衝擊荷重下之動態力學行爲進行發表，會議的過程中透過與其他與會學者討論研究心得並吸取其研究經驗後，使本人深覺獲益良多。未來無論是進行理論分析或實驗研究仍有非常大的發展空間，經過此次會議之發表，使筆者對未來之研究亦更具信心，並且對於後續之研究將秉持一貫之態度，接研究成果轉投於期刊論文，期望對相關領域研究在質與量上之提升能有所助益。

建議

本次參與會議後，筆者意識到結構與材料之動態反應與性質在民生工業、國防科技及防撞結構設計上日益重要，應用亦越來越廣。尤以今

年南台灣遭逢莫納克風災後，如何從材料與結構設計之角度，來提升重要民生設施與公共工程對落石、土石流等之耐衝擊性能，將是未來可思考之議題。另從鄰近國家如中國、日本、韓國及新加坡等國家對於參與此類之學術活動相當熱烈，其中以日本、中國及新加坡近年來在結構衝擊與爆炸防護等方面所投入的研究人力與經費可謂十分龐大，同時亦有多篇論文是透過國際合作研究共同完成的。反觀國內近年來雖然不斷的規劃國際合作研究、短期進修及各項國際研討會的補助，立意甚佳，然而若能在補助之員額及經費上再予以提升，除可增加學者之知識領域、拓展研究層次外，亦可將國內相關領域之研究狀況推廣於國際。

附 錄

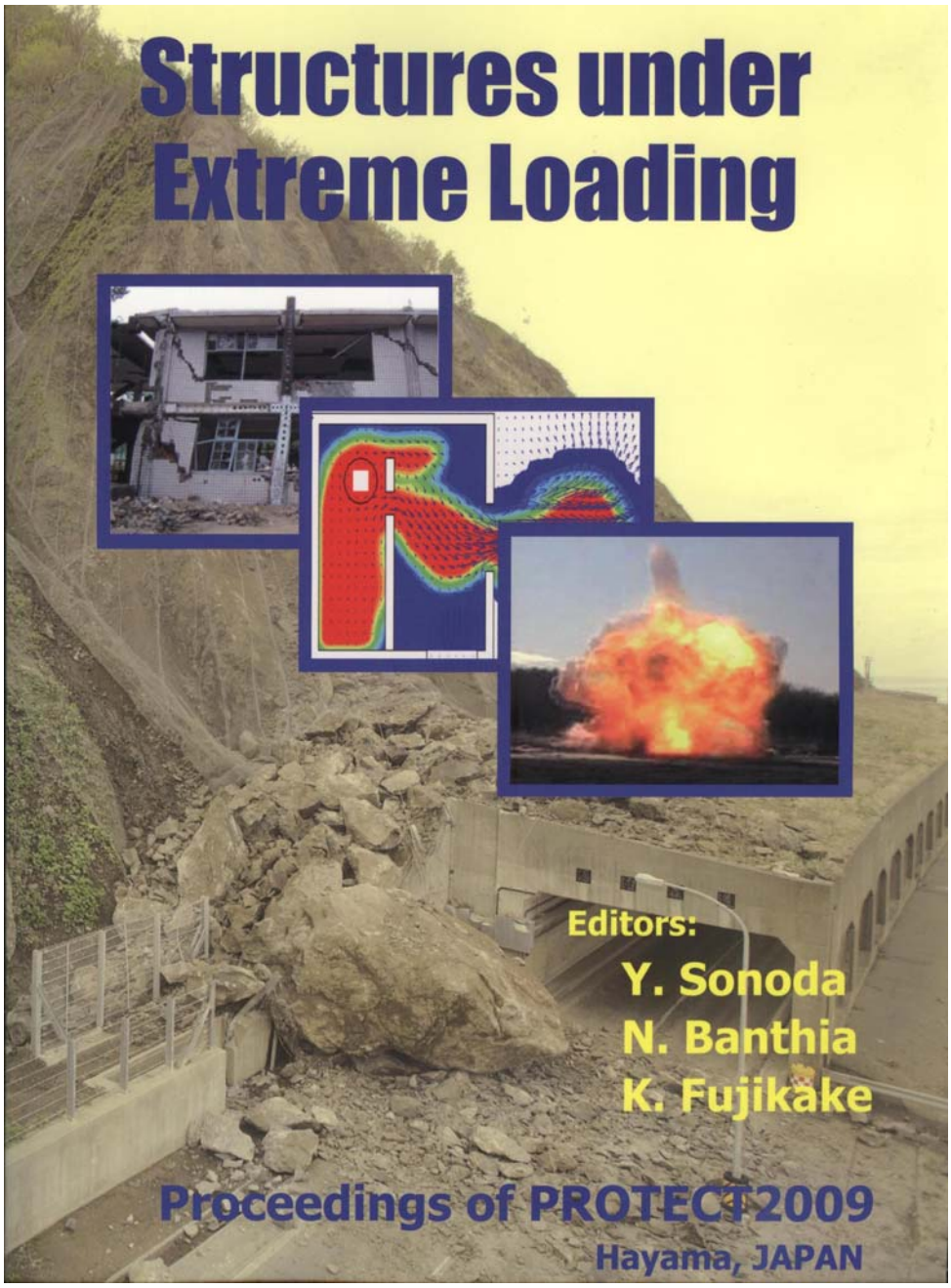
Structures under
Extreme Loading
Editors:
Y. Sonoda
N. Banthia
K. Fujikake
Proceedings of PROTECT2009
Hayama, JAPAN

MECHANICAL BEHAVIOR OF HIGH-STRENGTH CONCRETE AND ULTRA-HIGH STRENGTH CONCRETE UNDER REPEATED IMPACT LOADING

C.Y. Jen*

ROC Naval Academy, Taiwan, ROC

Abstract

The concrete is most widely used as the fundamental building construction material, so understanding the dynamic behavior of concrete under various conditions is an issue of great importance for applications in civilian and military engineering. In addition, the concrete material under the different strain rates and confinement effects, the behavior of mechanics is obviously different. Accordingly, the split Hopkinson pressure bar (SHPB) technique is used to examine the dynamic mechanics behavior of RPC under uni-axis and multi-axis stress. In addition, the mechanics performance of the reactive powder concrete under the static and dynamic loading is summed up completely and the results of this study can be utilized as a reference in research and design.

Keywords: steel fiber reinforced concrete, repeated impact, Hopkinson Pressure Bar test

* Corresponding author. Tel.:+886 7 5834700; Fax: +886 7 5834861.
E-mail address: cyjen@mail.cna.edu.tw (Chan-Yung, Jen).
Department of Marine Mechanical Engineering, ROC Naval Academy, Tsoying, Kaohsiung 813, Taiwan, Republic of China

1 Introduction

Concrete is the most commonly used construction material worldwide, which, during its working process, is frequently subjected to quasi-static loadings of magnitudes that change slowly. Designs of such large structures as nuclear power plant protection devices, airport runways and military facilities must however account for the impact of dynamic loadings of drastically changing magnitudes. Consequently, the materials chosen must resist shock and penetration and have high capacity for energy absorption. Concrete is typically comprised of cement, aggregate, water and an additive mixed according to a fixed ratio. As common concrete is known for its high compressive strength and low tensile strength, it is typically employed for its compressive strength, while the tensile strength is achieved by the use of steel bars. Whether a reinforced concrete component can be used effectively is largely dependent on whether concrete and steel bar deformation can be effectively transferred. Under quasi-static loadings, this criterion can be satisfied. However, under dynamic or shock loading, this criterion cannot be satisfied easily, mainly because such loading is generally local and stress is transmitted within the material as stress waves, which generate reflection within the concrete and at the interface where compressive waves become tensile waves. The fact determining the stress distribution inside reinforced concrete is difficult complicates the design process. The conventional design approach uses a high concentration of steel bars at various locations in the concrete, which increases cost and construction difficulty. For improving this property, high-strength steel-fiber concrete was developed. This concrete mainly consists of disoriented steel fibers added when mixing concrete. Various treatment methods have been employed to enhance compressive and bending strength, as well as fatigue and breaking resistance. The application of steel-fiber concrete, therefore, has garnered the attention of researchers [1–7]. In addition to typical civilian and infrastructure projects, steel-fiber concrete has shown great promise for securing military structures. A notable example is (SIFCON), which was developed by Lankard [8]. When creating SIFCON, flowing mortar is injected into a steel fiber skeleton situated in the false work. High-strength steel-fiber concrete contains 5–20% of steel fibers in mass. Experimental results indicate that SIFCON, due to the large amount of steel fibers, has significantly enhanced compressive and tensile strength. Especially noteworthy is that its toughness and ability to absorb energy are about 60 times greater that those of conventional concrete. Hackman *et al*. [9] studied (SIMCON), the basic materials and construction process of which are similar to those of SIFCON. The major difference between SIMCON and SIFCON is that the steel fiber net in SIMCON is formed by profiling molten iron and placing it in layers. The thickness of the steel fiber net is typically 13–50mm. Experiment results demonstrate that when the volume fractions of steel fibers in SIMCON is 12% of that in SIFCON, bending strength can reach 50% of that of SIFCON. Reducing the amount of steel fibers significantly

reduces cost. Richard *et al*. [10] developed Reactive Powder Concrete (RPC), and divided RPC into RPC200 and RPC800 based on strength. The enhanced strength of RPC is achieved by an improved mixing technique and treatment method that markedly increase the compression strength of concrete by 170–230MPa. After adding steel aggregate and applying a pressure of 50MPa before solidification, the strength of RPC800 can be as high as 800MPa. Although the special technical requirements make its application increasingly challenging, it has opened a door for new concrete research.

In this study, the split Hopkinson Pressure Bar (SHPB) test was extended for repeated impact testing of specimens with different steel-fiber volume fractions and examining the dynamic responses of different specimens under repeated impact, including fracture mode, during which damage accumulates. Results of this study provide a valuable reference for the research and design of concrete.

2 Experimental program

2.1 Materials

To explore the dynamic properties of high-strength steel-fiber concrete, this study of high-strength concrete and ultra-high-strength concrete specimens uses ASTM II Portland cement, silica fume (0.1–0.2μm), coarse and fine aggregate, quartz sand, quartz powder (5–25μm) and steel fiber. The fiber tensile strength is 2537MPa, and the length and diameter of fibers were 12.0mm and 0.175mm, respectively. To improve slurry at low water-cement ratios, a high-performance water-reducing agent was added during mixing. The chemical ingredient in the agent that is acrylic graft polymer anionic high molecular surfactant. Table 1 presents the specimen mixture.

Table 1: Concrete Mix (kg/m^3)

Specimen No.	w/(c+sf)	cement	water	cilica fume	coarse aggregate	fine aggregate	quartz sand	quartz powder	steel fiber	superplasticizer
HSC-F1	0.2	675	150	75	971	514	---	---	80	21
HSC-F2	0.2	675	150	75	944	514	---	---	160	30
UHSC-F1	0.2	750	185	179	---	---	969	189	80	40
UHSC -F2	0.2	750	185	179	---	---	942	189	160	40
UHSC -F3	0.2	750	185	179	---	---	916	189	240	40

2.2 Mixing proportions and specimen casting

Concrete mixes were prepared using a Hobart-type laboratory mixer with a capacity of 0.15 m^3. Cement, quartz fume, silica fume and silica sand were mixed first, and then water containing the appropriate amount of water-reducing agent was added. Steel fibers were added during the final mixing stage. Fibers were added to concrete at 80, 160 and 240 kg

per cubic meter of concrete; the densities are equivalent to 1.0%, 2.0% and 3.0% by volume of concrete. One-third of the water-reducing agent was added during the final 3 min of mixing. Molds were oiled and placed on a vibration table vibrating at a low speed while the concrete was poured. After each mold was filled, vibration speed was increased to ensure good compaction. Following casting, specimens were covered with a plastic membrane to prevent moisture evaporation and were stored in the laboratory at 25°C for 24 h; samples were then de-molded and placed in a thermostat-controlled water tank at 90°C for curing for 96 h. Finally, specimens were removed and stored at room temperature until testing after 28 days.

2.3 Experimental steps

Prior to impact tests, this study performed a quasi-static compression test for each set of specimens. Quasi-static compressive tests were performed in a closed loop, servo-controlled MTS810 test machine with a capacity of 1000 kN (Fig. 1). Prior to testing, the ends of each specimen were ground until parallel. The stress-strain curves were plotted using a strain gauge with a gauge length of 30mm; the gauge was attached to the test specimen to monitor axial deformations. During the experimental process, displacement was controlled and loading rates were 0.05 mm/min. Finally, maximum compressive strength and the stress-strain curve of each specimen were determined.

For dynamic testing, this study used the SHPB test device for repeated impact tests, in which the elastic responses of different specimens under repeated dynamic loadings, as well as the fracture mode of accumulated damage, were examined. Specimens HSC-F1, HSC-F2, UHSC-F1, UHSC-F2 and UHSC-F3 were tested and assigned different codes (R-). For example, the response of specimen UHSC-F3 under the third impact is represented by UHSC-F1-R3. In the experiment, the gas pressure within the high-pressure steel bottle was controlled via a control system and pressure valve; thus, when the projectile was fired and hits the input bar during each test, the magnitude of the strain wave generated and action time remain identical. During repeated impacts, the number of impacts and strain signal of the elastic bar after each impact were recorded.

Figure 1 Quasi-static test machine

3 SHPB test principle

To study the mechanical properties of materials under dynamic loadings, the SHPB test device was used most frequently. Since it was first developed by Kolsky[11] in 1949, the SHPB device has been the primary method employed by researchers for dynamic testing, primarily because the SHPB device has the following characteristics. (1) The test process is simple. The stress-strain relationship of the specimen is determined via strain signals of the two elastic bars. Since one does not need to measure the signal from the specimen, specimen destruction does not affect data acquisition. (2) The loading wave form can be controlled easily. The characteristics of dynamic loading differ from those of static loading. The loading method affects; thus, the geometrical conditions and mechanical properties of a specimen influence test results. The SHPB device uses the input bar to measure the incident and reflection waves, the difference between which is the impact loading acting on a specimen. Furthermore, when a projectile slides along the barrel at speed V and hits the input bar, a stress impulse $\sigma_I(t)$ resembling a rectangle is generated in the input bar. The amplitude of this stress impulse $(=\rho CV/2)$ can be controlled by adjusting impact velocity, V. Acting time is the time $(=2L_B/C)$ required for the projectile stress wave to travel back and forth once. Therefore, control can be achieved by adjusting the projectile length. In this manner, the strain rate of the specimen can be controlled and the stress-strain relationships under different strain rates explored.

3.1 Basic Assumption

The SHPB experiment primarily utilizes one-dimensional wave propagation theory. During the experiment, both the input and output bars must remain elastic, the length-to-diameter ratio of the bars must be appropriate, and the following assumptions must be met [11–14]:

(1) Wave propagation in the bar meets the hypothesis of one-dimensional stress wave propagation theory.

(2) Stress-strain relationship of the specimen is evenly distributed longitudinally.

(3) Lateral inertial effect is ignored.

According to the theory of one-dimensional stress wave propagation, the expressions of stress, strain and strain rate of the specimen can be simplified as

$$\dot{\varepsilon}_S(t) = -\frac{2C}{l_S}\varepsilon_R \tag{1}$$

$$\varepsilon_S(t) = -\frac{2C}{l_S}\int_0^t \varepsilon_R dt \tag{2}$$

$$\sigma_S(t) = \frac{A}{A_0}E\varepsilon_T \tag{3}$$

where $C = \sqrt{E/\rho}$ is elastic wave velocity of the bar; E and p are the elastic modulus and mass density of the bar, respectively; ε_R is the reflected wave; ε_T is the transmitted wave; l_S is the specimen length; and A the cross-sectional area of the elastic bar. By using Eqs. (1)–(3) with the time parameter eliminated, one can obtain the dynamic stress-strain curve under a high strain rate.

According to the energy conservation principle, the energy absorption density of a specimen can be determined by calculating the change in input energy and output energy:

$$E_s = \frac{1}{V_s}(E_I - E_R - E_T) \tag{4}$$

where V_s is specimen volume; E_I, E_R and E_T are incident energy, reflected energy and transmitted energy, respectively, which are expressed as

$$E_I = \frac{A}{\rho C}\int \sigma_I^2(t)dt \tag{5}$$

$$E_R = \frac{A}{\rho C}\int \sigma_R^2(t)dt \tag{6}$$

$$E_T = \frac{A}{\rho C}\int \sigma_T^2(t)dt \qquad (7)$$

Figure 2 shows the SHPB test device used in this experiment. The striker, incident pressure and transmitter bars are made of ANSI tool steel with a Young's modulus of 212.8 MPa. The striker, incident pressure and transmitter bars have identical diameters of 50 mm and lengths of 500.0, 1600.0 and 1600.0 mm, respectively. The end surfaces of the bars were lubricated to reduce friction. The axial impact of the striker bar and incident bar generates a compressive pulse, which is partially reflected when reaching the specimen between the incident bar and transmitter bar. The remaining portion of the wave is transmitted to the transmitter bar. The strain corresponding to the incident, reflected and transmitted pulses may then be measured using the strain gauge mounted on the bars connected via a Wheastone bridge. These signals, recorded by an oscilloscope and data-acquisition system, can be used to derive the corresponding strain pulses. For measuring the transient strain impulse, this study employs the strain gauge produced by KYOWA—gauge length is 5mm, resistance is 120 and signal rise time is roughly 0.89 μs. These properties are line with study requirements.

The oscilloscope in the SHPB impact test acquires the voltage signal. By rating the dynamic signal and the voltage-strain conversion via the calibrating voltage, one can determine the strain-time relationship of the incident wave, reflected wave and transmitted wave. Typical incident, reflected and transmitted waves corrected are shown in Fig. 3. Equations (1)–(3) yield the stress-strain curve and average strain rate.

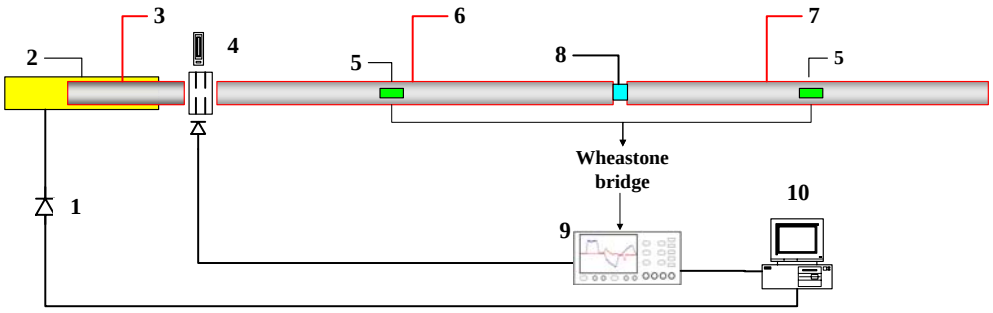

1: high-pressure air; 2: projectile guide barrel; 3: projectile; 4: grating velocity detection device; 5: strain gauge; 6: input bar; 7: output bar; 8: specimen; 9: signal amplifier and oscilloscope; 10: control box and data storage/analysis system

Figure 2 A schematic of the split Hopkinson pressure bar apparatus

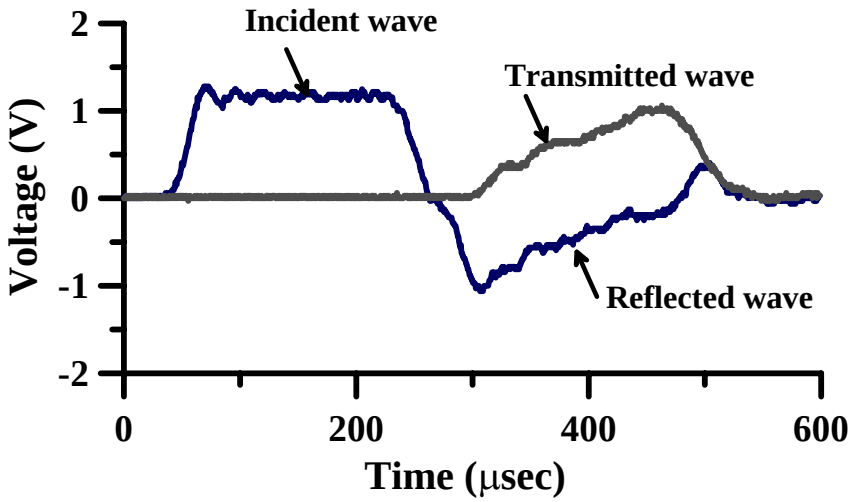

Figure 3 Typical waves from the incident and transmitted bar

3.2 Dispersion correction

The principal objective of dispersion correction is to transform strain gauge signals from the location of measurements back to the specimen-bar interface via a Fourier transform and dispersion equation. The method for dispersion correction— developed by [14]—is summarized as follows.

(1) Determine the number of Fourier components to be used in the frequency domain.

(2) From a digitized time-domain pulse, determine the total number of points that represent the pulse to be analyzed. In the Fast Fourier Transform (FFT) numerical scheme, the total number of sample points should be a power of 2 to minimize numerical operations.

(3) Calculate phase velocity and wave speed, c_0.

(4) Derive the amplitude and phase angle of each Fourier component.

(5) Determine the phase angle difference due to wave propagation along a distance x

(6) Convert the signal back into the time domain to obtain the corrected pulse.

4 Results and Discussion

4.1 Quasi-static test results

Table 2 lists the quasi-static mechanical testing results. When the steel-fiber volume fraction is 1%, the compressive strength of the HSC-F1 specimen is 109.5MPa, and relative strain is 0.35%. When 2% steel-fiber is added, compressive strength of the HSC-F2 specimen is 101.9MPa. For UHSC specimens, the compressive strengths are 139.7MPa, 157.4MPa and 190.1MPa after adding 1%, 2% and 3% steel-fiber, respectively, and the stress and strain of maximum strength increase significantly. Figure 4 shows the stress-strain curves of all specimens.

Table 2 : Mechanical Properties of HSC and UHSC

Specimen No.	Elastic Modulus (GPa)	Compression Strength (MPa)	Strain of Ultimate Strength (%)
HSC-F1	33.0	109.5	0.35
HSC-F2	33.9	101.9	0.29
UHSC-F1	48.5	139.7	0.26
UHSC -F2	48.7	157.4	0.34
UHSC -F3	44.3	190.1	0.49
UHSC –F2-R5	37.8	147.4	0.55
UHSC -F3-R5	39.7	172.0	0.53

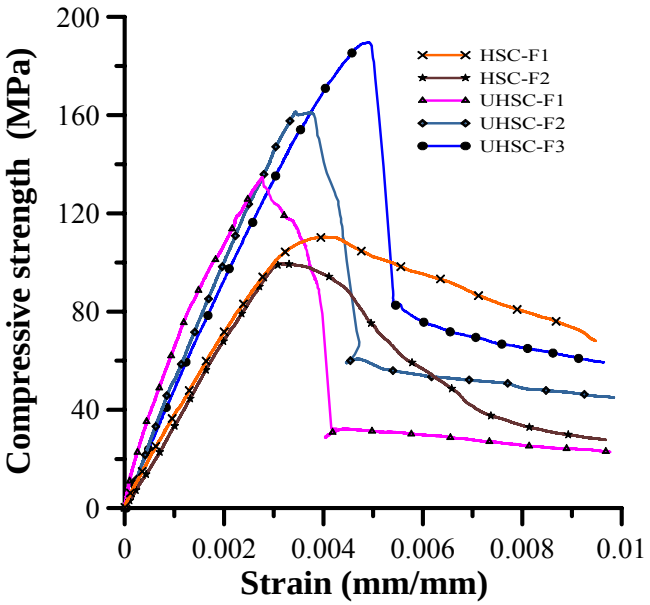

Figure 4 Stress-strain curve of specimens HSC and UHSC

4.2 Dynamic test results

Table 3 and Figs. 5–17 shows the dynamic mechanical property test results. Table 3 shows the experimental results of repeated impact testing. All tests are conducted under the condition that air pressure in the high-pressure steel bottle is <2kg/cm^2. Under this condition, the projectile speed is roughly 11.0m/sec. The actual velocity of the impact lever after each impact, however, is still measured by the grating speed detection device and oscilloscope. For the HSC-F1 specimen, damage is generated by the first impact; Fig. 5 shows the fracture mode. Figure 6 shows the stress-strain curve of the specimen under quasi-static and dynamic loadings. As concrete is a compound material made by mixing aggregate of different grades and cementing material, air in the mixing process forms pores inside specimens. Additionally, during the solidifying contraction process of the concrete, contraction of the aggregate and cementing material differ. Consequently, a

weakened transitional phase exists in the interface. A large number of micro cracks also exist in the area, resulting in microscopic heterogeneity of the material. The fracture process, therefore, can be considered the outcome of the combined effect of strain rate hardening (enhancing compressive strength and reducing corresponding strain) and damage softening. In the initial loading stage, damage is less significant than that during additional loading, and the major response is from the effect of strain-rate hardening. The compressive strength and initial elastic modulus increased from the quasi-static state (Fig. 6). As loading increases, material internal damage increases. When no steel-fiber is in a specimen or when volume fractions of the steel fibers are relatively low, a large number of micro cracks extend along the weakness band and form a damage transition zone, eventually resulting in specimen fracture.

Figure 7 shows the stress-strain relationship of the HSC-F2 specimen under two repeated impacts. Since the bridging effect of the steel fiber increases stress, the decline in residual strength of the specimen slows, reflecting the toughness of steel-fiber concrete. The same specimen was destroyed by the second impact. A comparison of the experimental results of the two impact tests indicates that the stress of the second impact is greater than that of the first impact, primarily because action time of the rectangular wave of the impact is two times the striker bar— is $195\mu\sec$. According to the strain rate over time for the specimen subjected to two repeated impacts (Fig. 8), maximum strain ($\dot{\varepsilon}=0$) of the specimen occurs when stress peaks at about $215\mu\sec$, indicating that after loading is removed, deformation continues and then the compressed part bounces back. Following the second impact, increased peak stress is mainly due to strain rate hardening. According to the study by Bischoff *et al*. [14], compressive damage of concrete results from development of unstable micro cracks. When loading speed is high, inertial resistance is increased by the bridging effect, and cracking speed peaks or the steel fiber crosses both sides of the cracks, resulting in delayed deformation and increased dynamic strength during loading. This phenomenon can be seen from the strain over time (Fig. 8). Figure 9 shows the fracture mode. Figure 10 shows the stress-strain curve of the UHSC-F1 specimen after two repeated impacts. Its overall reaction trend resembles that of the HSC-F2 specimen. Figure 11 shows the fracture mode of UHSC-F1 specimen.

Table 3: Summary of Repeated Impact Test

Specimen No.	Quasi-static Compression Strength (MPa)	Specimen Size	Impact velocity* (m/s)	Incident Energy E_I (J)	Reflected Energy E_R (J)	Transmitted Energy E_T (J)	Energy Absorption E_S (J)	Energy Absorption Ratio (J/cm^3)
HSC-F1	109.5	ϕ 50×98.8	10.7	424.4	96.1	106.6	221.7	1.14
HSC-F2	101.9	ϕ 50×98.8	11.5	500.1	96.1	134.3	269.8	1.39
			10.7	417.2	157.3	38.75	221.2	1.14
UHSC-F1	139.7	ϕ 50×98.5	10.9	435.1	74.7	159.8	200.6	1.04
			10.9	435.9	63.5	132.2	240.3	1.24
UHSC-F2	157.4	ϕ 50×97.5	10.8	429.0	58.6	244.5	125.9	0.66
			10.6	408.9	45.4	276.8	86.7	0.45
			10.4	401.8	48.5	290.3	63.1	0.33
			10.7	416.5	54.4	280.3	81.8	0.43
			4.9**	87.3	26.9	32.3	28.1	0.15
UHSC-F3	190.1	ϕ 50×97.9	10.8	434.2	58.5	181.5	194.3	1.01
			10.9	443.0	54.6	312.3	76.2	0.40
			10.7	419.5	51.2	255.9	112.4	0.59
			10.8	430.8	56.8	287.2	86.8	0.45
			10.6	419.2	54.6	233.4	131.3	0.68

Note: * The pressure of the high-pressure steel bottle is kept under 2kg/cm^2. Velocity of the projectile measured by the grating velocity detection device.
** Triggered when the aeration is incomplete.

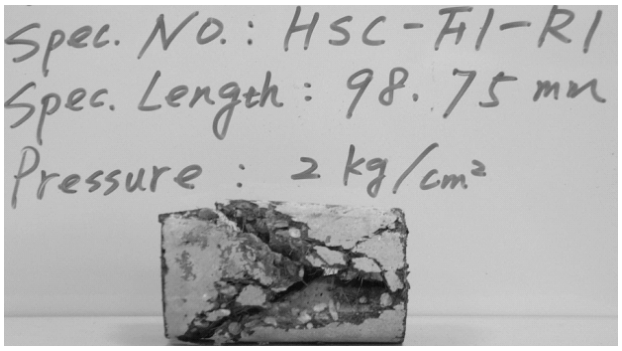

Figure 5. Fracture mode of HSC-F1 specimen after one impact

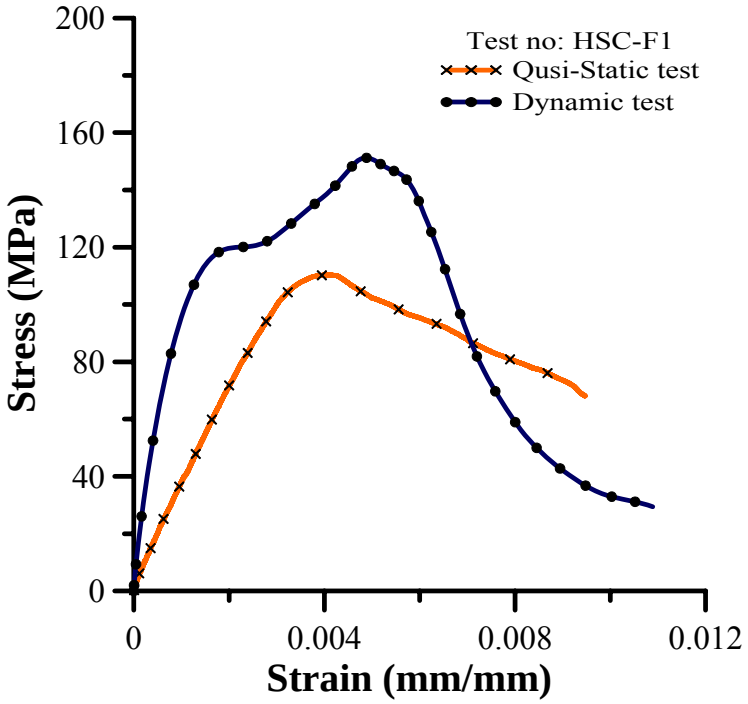

Figure 6. Stress-strain curve of HSC-F1 specimen under quasi-static and dynamic loadings

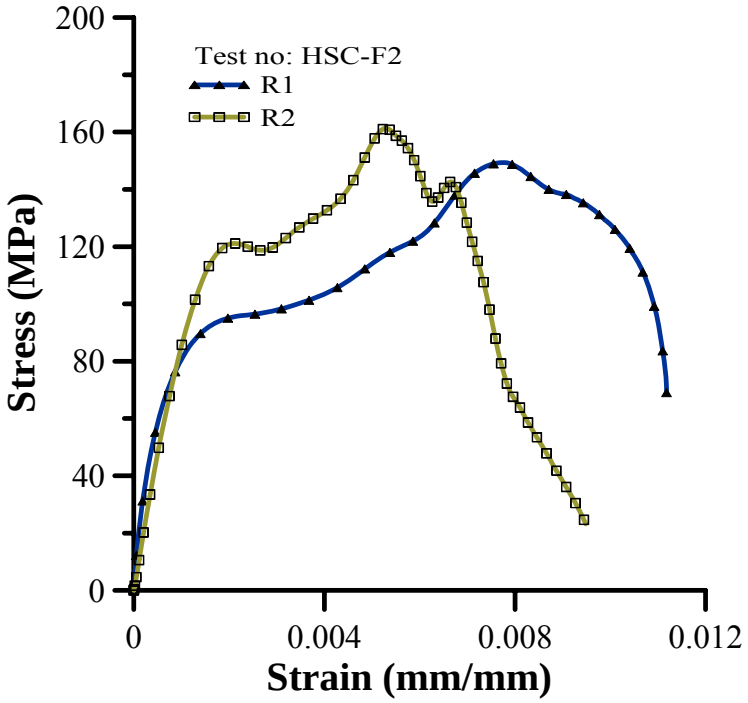

Figure 7. Stress-strain curve of HSC-F2 specimen under repeated impact

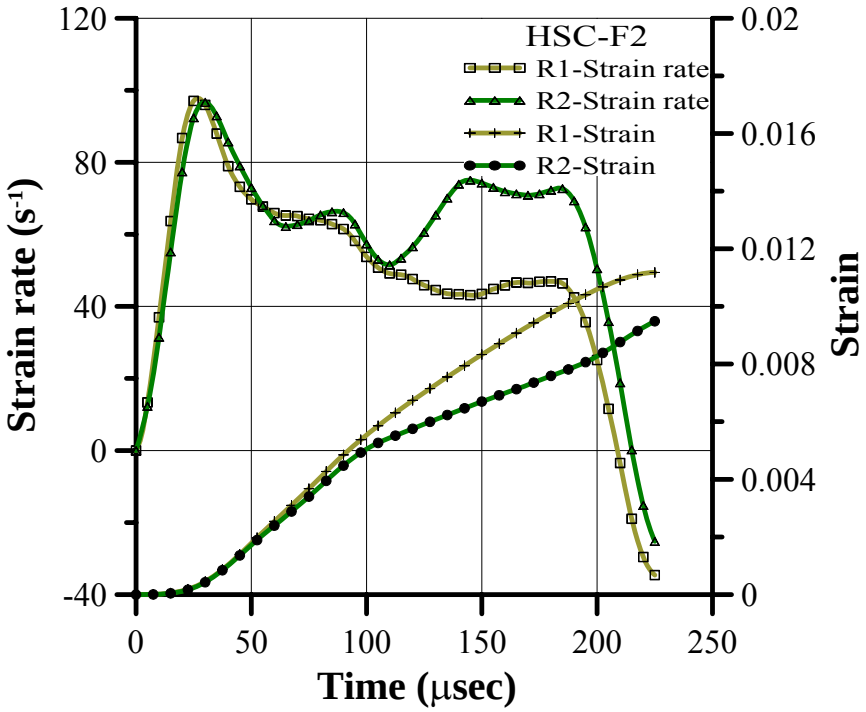

Figure 8. Strain rate and strain history of HSC-F2 specimen after two repeated impacts

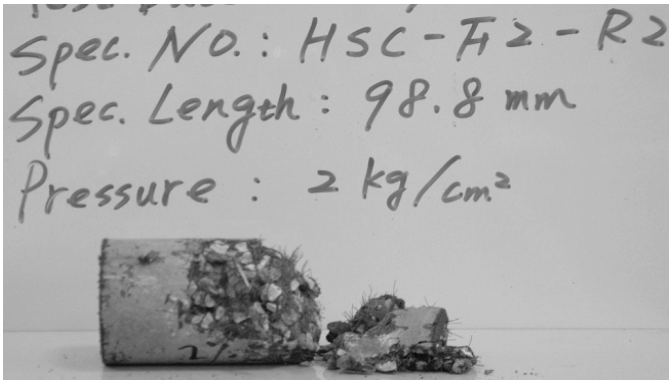

Figure 9. HSC-F2 specimen after two impacts

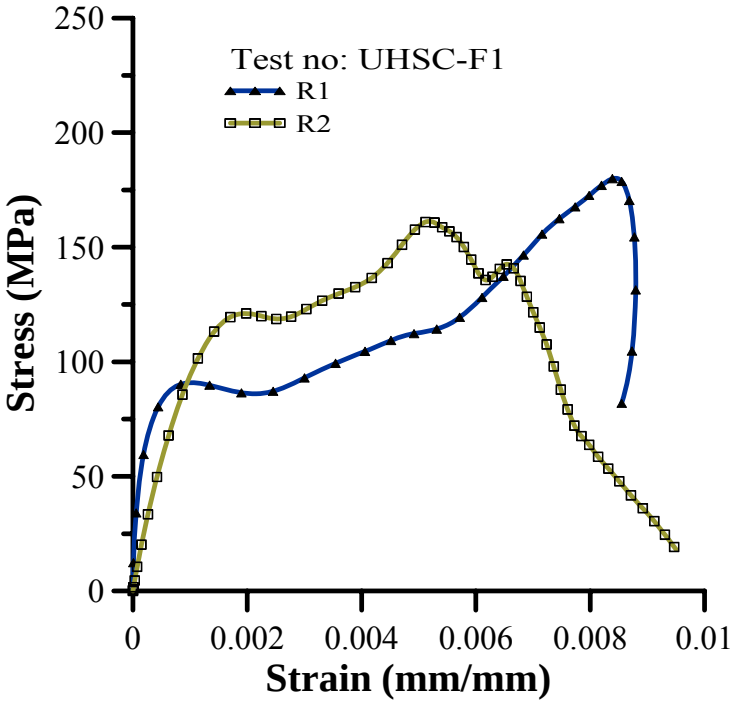

Figure 10. Stress-strain curve of UHSC-F1 specimen under repeated impacts

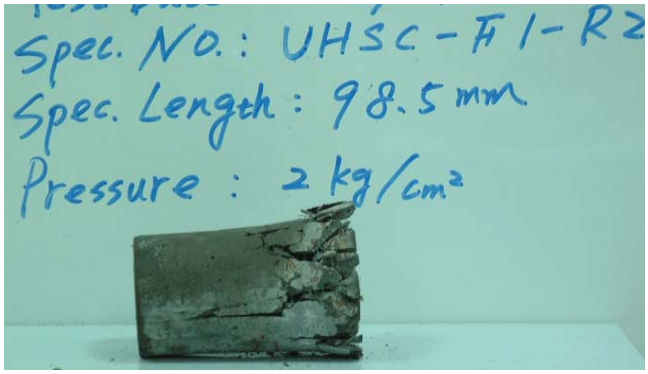

Figure 11. UHSC-F1 specimen after two impacts

Figures 12 and 13 show stress-strain curves of the UHSC-F2 and UHSC-F3 specimens under repeated impacts, respectively. The responses of these two specimens are identical; that is, stress under the first impact is smaller than that of the ensuing reaction. Thus, intensity gradually decreases as the number of impacts increases. However, as the quasi-static compressive strength of these two specimens is higher than that of other specimens, and the fiber volume fractions of specimens are 2% and 3%, respectively, the bridging effect of steel fibers significantly increases binding stress. Therefore, under such a stress wave, the UHSC-F3 specimen shows no obvious damage (Fig. 14). Furthermore, the slopes (dynamic elastic modulus) of initial loading of sections of the UHSC-F3 specimen under five repeated impacts are relatively consistent.

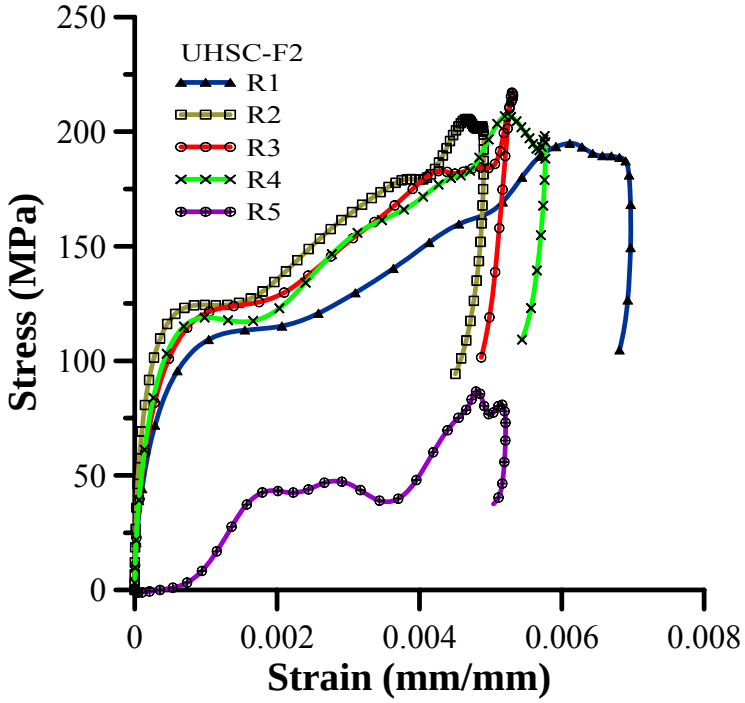

Figure 12. Stress-strain curve of UHSC-F2 specimen under repeated impact

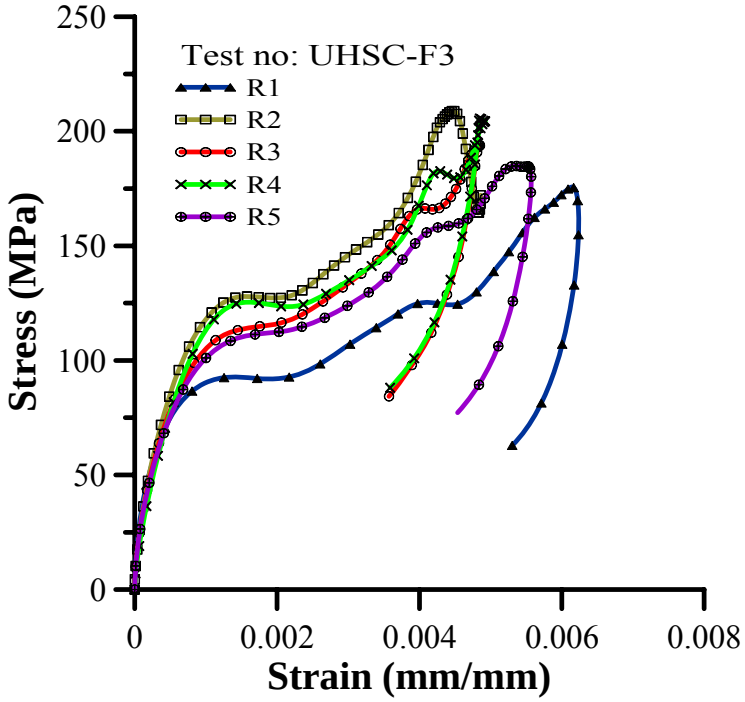

Figure 13. Stress-strain curve of UHSC-F3 specimen under repeated impact

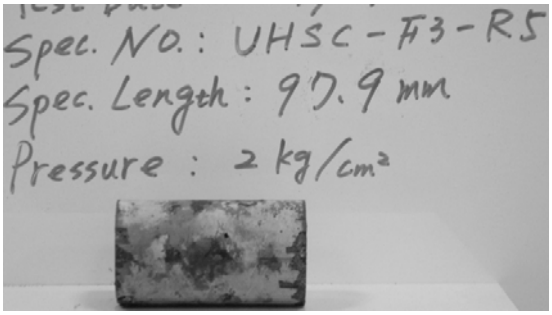

Figure 14. UHSC-F3 specimen after five repeated impacts

To quantify the internal damage of the two sets of specimens under this condition, this study tests the two sets of specimens following impact with a MTS-810 100 ton servo hydraulic machine. This test uses the same displacement control as that used in the quasi-static experiment, and has a loading speed of 0.05mm/min. Experiment findings demonstrate that the elastic modulus of the UHSC-F2 specimen remains 37.8GPa, and compressive strength is 147.4MPa; the elastic coefficient of the UHSC-F3 specimen remains 39.7GPa, and compressive strength is 172.0MPa. When the damage parameter is defined as $D = 1 - E_c / E_0$, where E_c and E_0 are post-stiffness declining elastic modulus and initial elastic modulus, respectively, the damage parameters for the UHSC-F2 and UHSC-F3 specimens are 0.23 and .0.10 respectively. Figures 15 and 16 The show the stress-strain curve changes of the two sets of specimens, respectively. Figure 17 shows the energy absorption per unit volume of all specimens accumulated during the impact process. Experimental results suggest that energy absorption of the UHSC-F3 specimen is 3.13J/cm^3, which is markedly superior to that of other specimens.

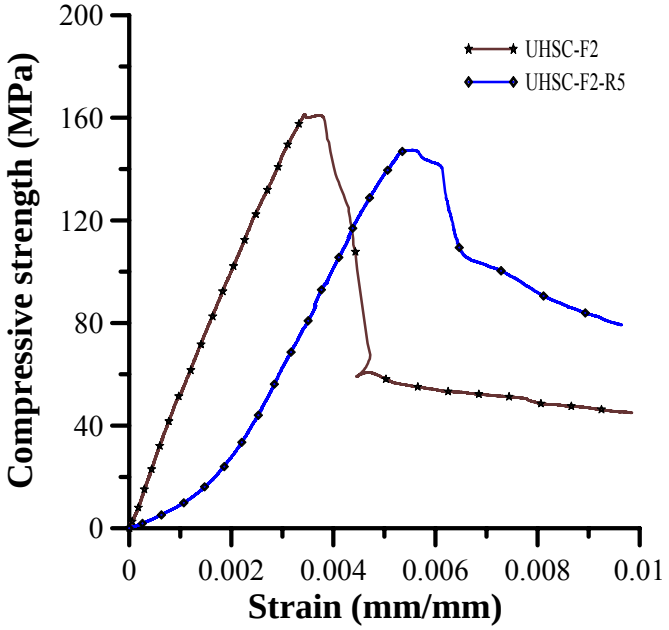

Figure 15. Comparison of mechanical properties of UHSC-F2 specimen before and after impact

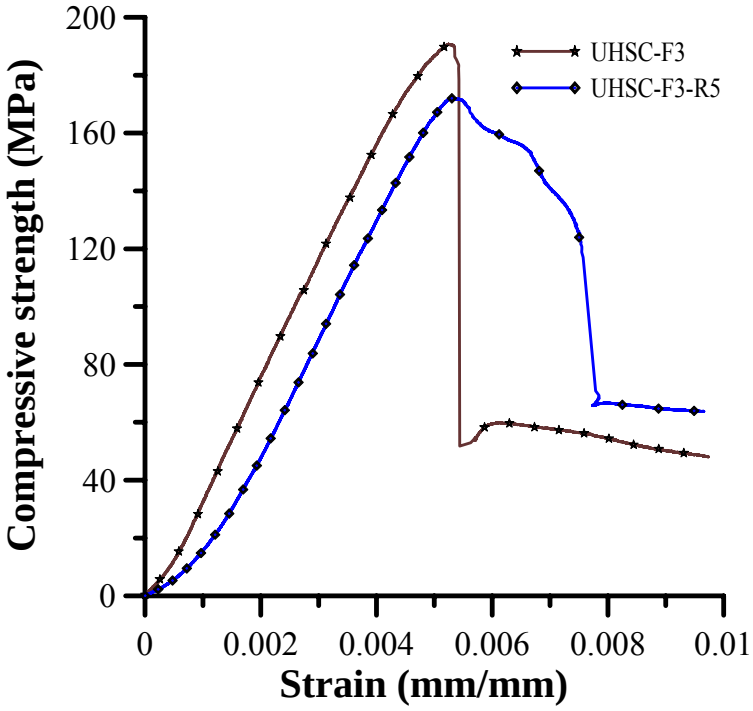

Figure 16. Comparison of mechanical properties of UHSC-F3 specimen before and after impact

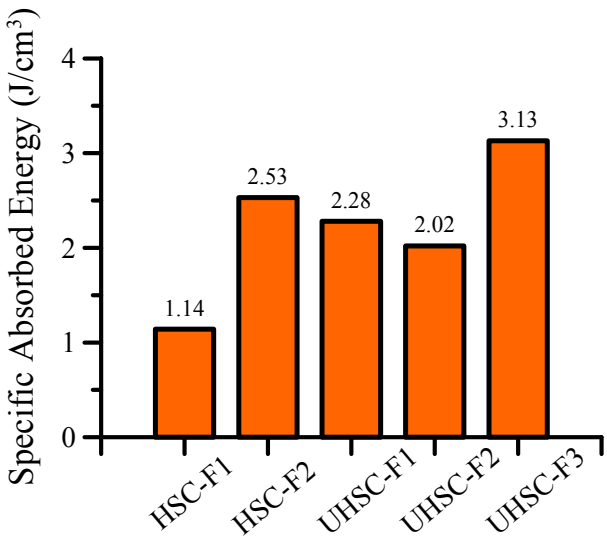

Figure 17. Energy absorption of different specimens under repeated impacts

5 Conclusions

Based on repeated impact tests of HSC and UHSC of this study, we conclude the following:

1. This study performed repeated impact tests for specimens with various steel-fiber volume rates using a SHPB test device. Experimental findings indicate that when a specimen is under dynamic loading, the destruction process can be considered the result of the combined effect of strain rate hardening and damage softening. During the initial loading stage, damage is less significant than that during subsequent loading, and the major reaction is due to the effect of strain rate hardening. As loading increases, material internal damage increases. When a specimen had no steel fibers or when the volume of steel fibers was relatively low, a large number of micro cracks extended along the weakness band, forming a damage transition zone, and eventually resulting in specimen destruction.
2. Compressive damage of concrete results from development of unstable micro cracks. When loading speed is high, the increase in inertial resistance is caused by the bridging effect and the fact that cracking speed peaks or steel fibers crossing both sides of the cracks, resulting in delayed deformation and an increase in dynamic strength during loading.
3. Under impact loadings, the dynamic energy absorption property of specimens is directly proportional to specimen strength and steel-fiber content. Experimental results suggest that the energy absorption of the UHSC-F3 specimen is markedly superior to that of other specimens.

References

1. Ramakrishnan, V., Coyle, W.V., Kulandaisamy, V. and Schrader, E.K. 1981. "Performance characteristics of fiber reinforced concretes with low fiber contents," J. Am. Concr. Inst. **78**(5): 388-94.
2. Shah, S. and Rangan, B.V. 1971 "Fiber reinforced concrete properties," J. Am. Concr. Inst. **68**(2): 126-35.
3. Balaguru, N. and Shah, S.P. "Fiber reinforced cement composites," New York, McGraw-Hill, 1982.
4. Ahmad, H.A. and Lagoudas, C.L. 1991 "Effective elastic properties of fiber reinforced concrete with random fibers," J. Eng. Mech. **117**(12): 2931–2938.
5. Banthia, N., Mindess, S. and Trottier, J.F. 1996 "Impact resistance of steel fiber

reinforced concrete," ACI Mater J. **93**(5): 472-479.

6. Banthia, N., Yan, C. and Sakai, K. 1998 "Impact resistance of fiber reinforced concrete at subnorma temperatures," Cement Concrete Comp. **20**(5): 393-404.
7. Wang, Z.L., Liu, Y.S. and Shen, R.F. 2007 "Stress–strain relationship of steel fiber-reinforced concrete under dynamic compression," Constr. Build Mater. doi:10.1016/j.conbuildmat..01.005.
8. Lankard, D.R. "Slurry infiltrated fiber concrete (SIFCON): properties and applications," *Materials Research Society Symposia Proceedings 1985*; **42**: 277-286.
9. Hackman, L.E., Farrell, M.B. and Dunham, O.O. 1992 "Slurry infiltrated mat concrete (SIMCON)," Concrete International: Design & Construction. **14**(12): 52-56.
10. Richard, P. and Cheyrezy, M. 1995 "Composition of reactive powder concretes," Cement and Concrete Research. **25**(7): 1501-1511.
11. Kolsky, H. "An investigation of the mechanical properties of materials at very high rates of loading," *Proc. Phys. Soc. 1949*, **B62**: 676-700.
12. Lindholm, U.S. 1964 "Some experiments with the split Hopkinson pressure bar," Journal of Mechanics of Physical and Solids. **12**: 317-335.
13. Davies, E.D.H and Hunter, S.C. 1963 "The dynamic compression testing of solids by the method of the split Hopkinson pressure bar," Journal of Mechanics of Physical and Solids. **11**:155-179.
14. Gong, J.C., Malvern, L.E. and Jenkins, D.A. 1990 "Dispersion investigation in the split Hopkinson pressure bar," Journal of Engineering Materials Technology, Transactions of the ASME. **112**: 309-14.
15. Bischoff, P.H. and Perry, S.H. 1995 "Impact Behavior of plain concrete loaded in uniaxial compression," Journal of Engineering Mechanics. **121**: 685-693.